

# What governs rivulet meanders on an inclined plane ?

Nolwenn LE GRAND-PITEIRA,\* Adrian DAERR, and Laurent LIMAT

*Laboratoire de Physique et Mécanique des Milieux Hétérogènes,  
10 rue Vauquelin 75005 Paris France, UMR CNRS 7636*

*and Matière et Systèmes Complexes, University Paris 7, UMR CNRS 7057*

(Dated: May 24, 2019)

We performed experiments on streams of water flowing down a Mylar substrate, for various plate inclinations and flow rates, and we focused on the regime of stationary meanders. We found that (i) the flow is highly hysteretic: the shape of the meanders varies with flow rate only for increasing flow rates, and the straight rivulet regime does not appear for decreasing flow rate. (ii) A simple model, including inertia and capillary forces, as well as hysteresis of wetting, accounts well for the experimental instability threshold as well as for the final radius of curvature of the meanders.

PACS numbers: Valid PACS appear here

Meanders are ubiquitous in nature and are most familiar from rivers, but can also be seen at a much smaller scale on rivulets flowing down inclined surfaces, as for instance on window-panes during a rainfall. Recently, Drenckhan et al. [1] have identified remarkably regular meandering patterns on rivulets confined between two vertical plates and charged with surfactants to mimic undulations of foam Plateau borders. This observation confirms the generality of this pattern, and suggests that a well defined mechanism is at work in rivulets, able to select a given meandering length scale. Understanding this mechanism and the properties of the resulting meanders is by itself a fundamental challenge, that can also have implications in other fields of physics. For instance Bruinsma [2] pointed out a possible analogy with the statistics of directed polymers inside a random matrix.

In the case of rivers [3, 4], it seems asserted that erosion is the key mechanism, but as opposed to this, the meandering on non-erodible surfaces is still an essentially open problem. Surprisingly, very few studies of meandering rivulets have been done. Culkin [7] and later Nakagawa and Scott [8] reported significant experimental work on streams running down an inclined plate. They identified three regimes for increasing flow rates: a drop regime, a meandering regime, and an unstable regime (the main rivulet oscillates and splits into several smaller ones). They also stress that they never obtain straight rivulets, though this regime has been reported by Schmuki and Laso [9] who also investigated the effects of viscosity and surface tension. Exploratory studies have been done on the unstable rivulet regime [9, 10]. Stability analyses of rivulets, some neglecting longitudinal flow [5, 6], are mainly focused on varicose modes and not sinuous modes, i.e. are not dealing with meandering instability. Only two recent papers deal with meandering threshold [2, 11].

Concerning technical applications, rivulets play an important role in aerospace industries, decreasing aerodynamic efficiency and controlling the pattern of ice formation on the wings of airplanes under freezing conditions [12]. In heat exchangers, the changes between differ-

ent flow regimes can cause drastic modifications of heat transfer [13]. Rivulet formation can also be an undesirable feature in coating processes [14], except for possible specific applications. Therefore, knowledge on their stability and characteristics would be of great help in optimizing several industrial processes.

This paper studies the shape and behavior of meandering rivulets as a function of our control parameters (flow rate and plate inclination), and discusses physical interpretations, focusing on the role of hysteresis.

*Experimental set-up* – Figure 1a shows a schematic diagram of the experimental set-up. De-ionized water is

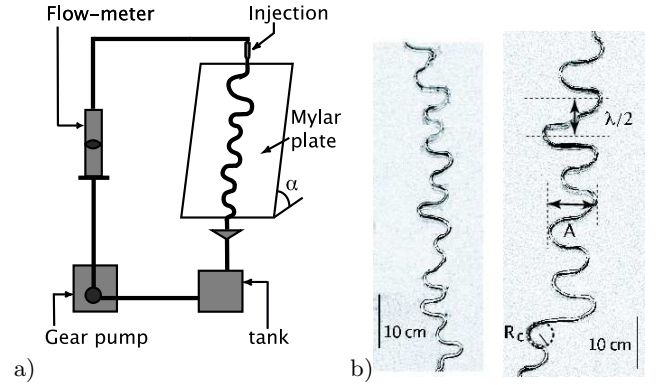


FIG. 1: a) Experimental setup b) Stationary meanders for  $\alpha = 32^\circ$ .  $Q=1.08$  mL/s for the left picture and  $Q=1.40$  mL/s for the right one.

injected at the top of an inclined plate (1.20 m long and 50 cm wide). The substrate is a Mylar sheet, flattened on a rigid plate, insuring partial wetting conditions for water (with advancing and receding contact angles of respectively  $\theta_a = 70^\circ$  and  $\theta_r = 35^\circ$ ) and also reducing problems of static electricity compared to other common plastics. The tilt angle  $\alpha$  of the plate can be changed at will between  $0^\circ$  and  $87^\circ$ . The water is collected in a tank and pumped back to the top of the plate by a gear pump providing an adjustable and constant flow rate  $Q$ . The

constancy of the flow rate is crucial in achieving stable meanders, and is checked through the use of a precision flow-meter. Pictures and movies of the experiments were taken by a digital camera placed 1 m above the plate and perpendicular to the latter.

*Meandering thresholds* – For increasing flow rates, the following regimes are observed. (i) Drops. Individual drops periodically detach from the injector [15]. (ii) Straight rivulets. The liquid flows down forming a straight continuous ridge along the direction of steepest descent. (iii) Meandering rivulets. Above a critical flow rate  $Q_{c1}$ , depending on the plate inclination, the straight liquid ridge is unstable. Perturbations (surface defects, injection noise, air movement, ...) appear as small bends of a typical size comparable to the rivulet width  $w$ . These bends initially amplify laterally and downwards but eventually reach a stationary shape. It takes 10 minutes to one hour for a rivulet to fully develop along the whole length of the plate, but then the resulting meander is completely stationary (Fig. 1b). Snapshots of a settled meander have been taken every 2 minutes during 24 hours, and it did not move at all throughout that time lapse. Using a highly steady pump, a carefully designed injector and a long support to check whether the behavior of the rivulet depended on the distance to the injector, we have been able to verify that meandering regime for rivulets does exist independently of injection conditions, confirming previous findings by other groups. (iv) Dynamic regime. Above a second critical flow rate  $Q_{c2}$ , meanders no longer remain stable. The rivulet sweeps from side to side below the injector similar to the free edge of a garden hose [16], frequently breaking up into sub-rivulets and running down along unsteadily changing paths.

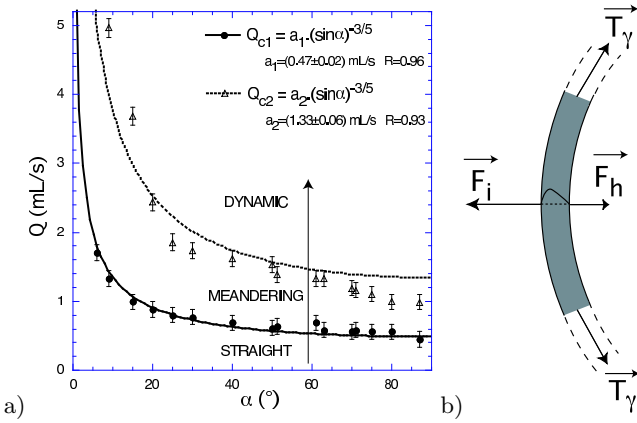


FIG. 2: a) Meandering thresholds for increasing flow rates b) Forces acting on a meander, in the plane of the plate

Figure 2a displays the dependency of the two criti-

cal flow rates on the plate inclination  $\alpha$ , for stationary meanders. The decrease of the second critical flow rate  $Q_{c2}$  with  $\alpha$  is similar to that of  $Q_{c1}$ , and we have no explanation for that yet. The dependency of  $Q_{c1}$  on  $\alpha$  can be understood from the balance of the forces acting on the rivulet: gravity, surface tension, inertia and contact line pinning forces. For the lateral stability of a straight rivulet gravity does not intervene (2b). The surface tension opposes the bending of the rivulet and, once integrated across the cross-section, can be seen as a line tension  $T_\gamma$  of the liquid rim [17]. This line tension creates a normal force  $F_\gamma$  straightening the rivulet, and taking into account the interfacial energies and the capillary pressure inside the rivulet, reads  $F_\gamma = C\gamma w/r_c$ , where  $C$  is a constant ( $C \approx \theta^2/3$  in the limit of a small average contact angle  $\theta$ ),  $\gamma$  the surface tension,  $w$  the width of the rivulet and  $r_c$  the initial radius of curvature. Pinning forces are reactive, therefore stabilizing forces, and act normal to the contact line. They have an upper bound given by the advancing and receding contact angles:  $F_h \leq F_h^{\max} = \gamma(\cos\theta_r - \cos\theta_a)$ . Instability will arise when inertia ( $F_i = \rho S v^2/r_c$  where  $\rho$  stands for the density of the liquid,  $S$  for the cross-section of the rivulet and  $v$  for the RMS velocity inside the rivulet) becomes stronger than both line tension and pinning ( $F_i \geq F_\gamma + F_h^{\max}$ ). The onset of meandering is therefore given by :

$$\rho \frac{Q_{c1}^2}{S r_c} = \gamma \left[ \frac{Cw}{r_c} + (\cos\theta_r - \cos\theta_a) \right] \quad (1)$$

Without the pinning term, this balance was also suggested by Drenckhan *et al.* [1] for their meanders in foams. If the pinning term can be neglected, or else if  $r_c$  scales as  $w$  with flow rate, the first critical flow rate scales as  $\rho Q_{c1}^2/S \propto \gamma w$ . Let us now assume that the flow inside the rivulet is a Poiseuille flow ( $v \propto w^2 g \sin\alpha/\nu$ , where  $\nu$  denotes the kinematic viscosity), and approximate the cross-section of the rivulet to a disc segment with  $\pi/4$  contact angle ( $S = w^2/8$ ). Using the flow rate conservation ( $Q = Sv$ ), leads to the scaling

$$Q_{1c} \propto \left[ (\gamma/\rho)^{4/5} (\nu/g)^{3/5} \right] (\sin\alpha)^{-3/5}, \quad (2)$$

which is plotted for comparison with the experimental findings in figure 2a, and seems to match the data fairly well, with a prefactor of order 1. This result is close to the one predicted by Bruinsma [2]. Rough estimates of the force terms in equation (1) using experimental data for typical threshold conditions show that pinning is not completely negligible [18]. The pinning term of equation 1 alone would lead to the scaling  $Q_{c1} \propto (\sin\alpha)^{-1/2}$ , so the apparent exponent is in fact expected to be in between  $-3/5$  and  $-1/2$ , which remains consistent with our data.

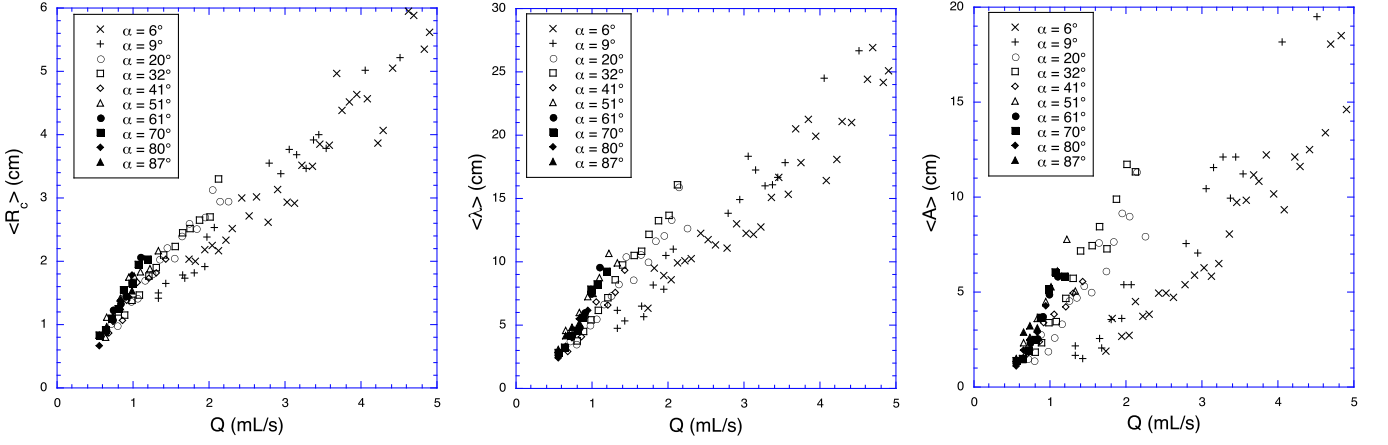


FIG. 3: Experimental data for the mean radius of curvature, wavelength and amplitude for numerous plate inclinations.

If the flow rate is now decreased when in the meandering regime, we observe a remarkable stability of the meanders: rivulets conserve their path, becoming thinner, until the rivulet breaks up into drops. In particular there is no sinuous/straight rivulet transition  $Q_{c1}$  and the rivulets meanders instead of becoming straight again below  $Q_{c1}$ . This strong hysteresis is a consequence of pinning effects. For all features of a meander with a radius of curvature greater than  $Cw/(\cos\theta_r - \cos\theta_a) \approx 2w/5$ , i.e. for all but very small scales, contact line pinning forces (now acting in the opposite direction) will dominate restoring capillary forces (cf. equ. (1)) even if inertial forces tend to zero.

*Shape of the stationary meanders* – All the experimental data presented here were obtained for increasing flow rates. For numerous meanders achieved for plate inclinations varying between  $6^\circ$  and  $87^\circ$ , we measured the mean radius of curvature  $\langle R_c \rangle$  at the apex of the curves (mean taken over all curves of a given rivulet), mean wavelength  $\langle \lambda \rangle$ , and mean amplitude  $\langle A \rangle$  (see figures 1b and 3). All three parameters increase monotonically with the inclination of the plate  $\alpha$  and the flow rate  $Q$ .

The magnitude of inertial and capillary forces depends on the shape of the rivulet path. The equilibrium of gravity, inertia, capillarity and pinning forces can therefore be used to solve for the expected radius of curvature of stationary meanders. Again, gravity does not matter if we are interested in the curvature at the vertical segments of the meander. The force balance at the threshold of depinning/motion then reads:

$$(\rho Q^2/S - C\gamma w)/R_c = \gamma(\cos\theta_r - \cos\theta_a) \quad (3)$$

This is the same as equ. (1) except that  $R_c$  is now the final radius of curvature of the bends in the meander.

An order of magnitude calculation [18] shows that the contribution of inertia  $\rho Q^2/S$  is bigger than the capillary

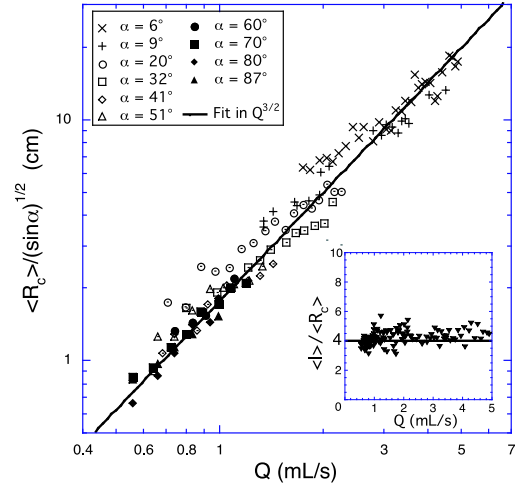


FIG. 4: Comparison of the data to the model for the mean radius of curvature. Insert: ratio of the wavelength to the radius of curvature for all plate inclinations  $\alpha$ .

contribution  $C\gamma w$ . We therefore neglect the latter, and assuming a Poiseuille flow, we get the following scaling law for the radius of curvature:

$$\langle R_c \rangle \propto \frac{\rho(g/\nu)^{1/2}}{\gamma(\cos\theta_r - \cos\theta_a)} Q^{3/2} \sqrt{\sin\alpha} \quad (4)$$

We have tested this expression on our data (Fig. 4) and the scaling law fits the data reasonably well.

Some sets of data, for a given inclination, seem to have a slightly different slope from the proposed scaling law. A first possible explanation lies in the neglected capillary term, which would add a contribution to the radius of curvature in  $-Q^{1/4} \sin^{-1/4}\alpha$ , which is more important at low inclinations and low flow rates, and diminishes the final radius. A second important point is the reduction of the effective slope through sinuosity  $\mathcal{S}$  (ratio of total length of the rivulet to the distance between

its endpoints). The slope  $\sin \alpha$  has to be replaced by  $\sin \alpha / \mathcal{S}$  in eq. (4), and since  $\mathcal{S}$  increases with  $Q$  and  $\alpha$  [8], the exponents of  $Q$  and  $\alpha$  should be smaller than the ones in equation 4. Last but not least, the Poiseuille flow assumption probably needs to be corrected. Indeed flow visualizations with methylene blue dye show regions with zero or even backward recirculating flow [19]. The Reynolds number based on the rivulet size is of order  $10^3$ , so some turbulence can be expected.

*Discussion* – The scenario for the development of meanders may be summed up as follows. Stable rivulets become unstable when inertia dominates capillary forces, through the amplification of perturbations (to be accurate, pinning forces have to be added to the balance). Because the destabilizing terms diminish as a perturbation grows (and so its radius), the hysteresis of wetting eventually re-stabilizes the perturbation. In the final state, the pinning forces should therefore be maximally mobilized, with the critical advancing contact angle on the outside of the curve and the critical receding contact angle on the inside. Cross-section measurements by Nakagawa and Scott [8] seem to corroborate this, but more quantitative measurements are planned.

As appears in figure 1b, the final meanders are made up of circular segments and the relationship  $\langle \lambda \rangle = 4 \langle R_c \rangle$  should be expected from meanders made of half-circles possibly followed by horizontal segments. This is confirmed by the insert in figure 4 plotting the ratio  $\langle \lambda \rangle / \langle R_c \rangle$  versus flow rate  $Q$ : the measurements are a bit scattered, but indeed close to 1.

In order to understand how the rivulet switches from one bend to the next, gravity has to be taken in account to explain why the rivulet does not follow the circular path back uphill. If weight is strong enough, it will exceed pinning at a critical orientation of the rivulet with respect to the slope,  $\sin \Phi = \gamma(\cos \theta_r - \cos \theta_a) / \rho g S \sin \alpha$ . If pinning always remains stronger, the rivulet can become horizontal without slipping. In the first case the critical orientation will define the inflection points on the path. In the second case, horizontal segments appear, in which the velocity decreases and the cross-section increases until gravity becomes dominant. Both scenarios seem to correspond to observed patterns, but the effect on the amplitude of the meanders is not clear.

A last point remains to be discussed: above  $Q_{c1}$  perturbations must be stabilized at large scales because the de-stabilizing forces decrease for smaller curvatures, but why do no new perturbations appear at small scales if we are above the threshold  $Q_{c1}$ ? The formation of a meandering path decreases the mean velocity: injection of some methylene blue dye into the rivulets revealed that the mean velocity of the flow drastically drops at the transition from straight-to-meandering. Therefore, the rivulet becomes stable in the meandering part, and remains unstable in the parts which have not yet developed bends. It would be interesting to perform velocity

measurements to see whether the second threshold  $Q_{c2}$  is defined by the same critical local velocity as  $Q_{c1}$ .

*Acknowledgments* –: We thank B. Andreotti and M. Argentina for stimulating discussions and B. Andreotti for a critical reading of the manuscript.

---

\* Electronic address: nlegrand@pmmh.espci.fr

- [1] W. Drenckhan, S. Gatz and D. Weaire, *Phys. Fluids*, **16**, 3115-3121 (2004).
- [2] R. Bruinsma, *J. Phys. France*, **51**, 829-845 (1990).
- [3] L.B. Leopold and M.G. Wolman, *Bull. Geol. Soc. Am.*, **71**, 769-794 (1960)
- [4] T.B. Liverpool and S.F. Edwards, *Phys. Rev. Lett.*, **75**(16), 3016-3019 (1995)
- [5] S. H. Davis, *J. Fluid Mech.*, **98**(2), 225-242 (1980); K. Sekimoto, R. Oguma and K. Kawazaki, *Ann. Phys.*, **176**, 359-392 (1987)
- [6] G.W. Young and S.H. Davis, *J. Fluid Mech.*, **176**, 1-31 (1987); R.V. Roy and L.W. Schwartz, *J. Fluid Mech.*, **391**, 293-318 (1999)
- [7] J. B. Culklin, *Ph. D. Northern University, Illinois*, (1982)
- [8] T. Nakagawa and J. C. Scott, *J. Fluid Mech.*, **149**, 89-99 (1984).
- [9] P. Schmuki and M. Laso, *J. Fluid Mech.*, **215**, 125-143 (1990)
- [10] T. Nakagawa, *J. Multiphase Flow*, **18**, 455-463 (1992).
- [11] H. Kim, J. Kim and B. Kang, *J. Fluid Mech.* **498**, 245-256 (2004)
- [12] J.S. Marshall and R. Ettema, *Proceedings of the Fifth Microgravity Fluid Physics and Transport Phenomena Conference*, 1217-1227, (2000)
- [13] E. N. Ganic and M. N. Roppo, *ASME J. Heat Transf.*, **102**, 342-346 (1980)
- [14] S. F. Kistler and P. M. Schweizer, *Liquid film coating - Scientific principles and their technological implications*, edited by Chapmann & Hall (1997)
- [15] N. Le Grand, A. Daerr and L. Limat, *J. Fluid Mech.*, **541**, 293-315 (2005)
- [16] S. Kuronuma and M. Sano, *J. Phys. Soc. Jpn.*, **72**, 3106-3112 (2003)
- [17] Two forces act normal on a transverse section of area  $S$  through the meander: pressure  $-S\Delta p$  and surface tension. The surface tension is made up of two parts: the water-air interface of length  $\ell$  contributes a term  $\gamma\ell$ , the straight mylar-water interface of length  $w$  (rivulet width) contributes a term  $-\gamma w \cos \theta$  corresponding to the energy difference of wet and dry mylar,  $\theta$  being an average contact angle. The effective rivulet string tension is  $T_\gamma = \gamma(\ell - w \cos \theta) - S\Delta p$ . Approximating the water-air interface by a circular arc of radius  $r$  intersecting the mylar-water interface at the equilibrium contact angle  $\theta$ , we find that  $\ell = 2\theta r$ ,  $w = 2r \sin \theta$ ,  $\Delta p = \gamma/r$  (neglecting the longitudinal rivulet curvature) and  $S = \theta r^2 - (1/2)wr \cos \theta$ . With these relations, the rivulet string tension becomes  $T_\gamma = (1/2)\gamma w(\theta/\sin \theta - \cos \theta) = C\gamma w$ .
- [18] For the contact angles given in the text, the pinning force is around  $F_h = 35 \text{ g.s}^{-2}$ . Inertial and capillary terms evaluate to  $\rho S v^2 = \rho Q^2 / S = 50 \text{ g.cm.s}^{-1}$  and  $C\gamma w = 6 \text{ g.cm.s}^{-1}$  for  $Q = 1 \text{ mL.s}^{-1}$ ,  $w = 4 \text{ mm}$ .
- [19] J. Walker, *Am. Sci.*, **253**, 132-137 (1985).